

Article

# The Development of a Highly Sensitive Fiber-Optic Oxygen Sensor

Cheng-Shane Chu \* and Jhih-Jheng Syu

Department of Mechanical Engineering, Mig-Chi University of Technology, New Taipei 24301, Taiwan; q29834542@yahoo.com.tw

\* Correspondence: cschu@mail.mcut.edu.tw; Tel.: +886-2-2908-9899

Academic Editor: Chien-Hung Liu

Received: 23 March 2016; Accepted: 28 April 2016; Published: 3 May 2016

**Abstract:** This paper presents a highly sensitive fiber-optic oxygen sensor. The sensor was fabricated using palladium (II) meso-tetrakis (pentafluorophenyl) porphyrin (PdTFPP) and porous silica nanoparticles embedded in a tetraethylorthosilane (TEOS)/n-octyl-triethoxysilane (Octyl-triEOS) composite xerogel present as a coating on the end of the fiber. Sensitivity is quantified in terms of the ratio  $I_{N_2}/I_{O_2}$ , where  $I_{N_2}$  and  $I_{O_2}$  represent the intensity of fluorescence detected in a pure nitrogen or pure oxygen environment. The experimental results reveal that this PdTFPP-doped oxygen sensor with porous silica nanoparticles has a sensitivity of  $I_{N_2}/I_{100O_2} = 386$ . The results also show that this sensor has higher sensitivity than an oxygen sensor based on Pd(II) complex immobilized in a sol-gel matrix. Furthermore, the optical oxygen sensor yields a linear Stern–Volmer plot. The proposed optical sensor has the advantages of easy fabrication, low cost, and high sensitivity to oxygen.

**Keywords:** fiber-optic oxygen sensor; PdTFPP; porous silica nanoparticles; sol-gel

## 1. Introduction

Oxygen plays an essential role as either a reactant or a product in many chemical and biochemical reactions. Consequently, many researchers have expended considerable effort in developing simple and low-cost techniques for the fabrication of high performance fiber-optic oxygen sensors. One of the earliest oxygen sensors was the Clark electrode, designed to measure the oxygen pressure in arterial blood samples [1]. Although the Clark electrode gives reasonably accurate results, its general applicability is limited. There are several reasons for this, the most notable of which are high oxygen consumption, slow response, poor reliability, and questionable safety [2]. Optical oxygen sensors have overcome the drawbacks of the Clark electrode and are now widely used in the chemical [3], clinical [4], and environmental monitoring [5] fields. Usually, these optical oxygen sensors consist of an analyte-sensitive dye in a supporting matrix. The oxygen sensors presented in the literature invariably use an embedded fluorescent dye in either a polymer [6] or an organically modified silicate (ORMOSIL) [7–12]. The ORMOSIL can accommodate and disperse oxygen-sensitive dyes and can also have a porous structure which is vital for rapid optical sensor response [13]. In addition, it has also been demonstrated that an ORMOSIL matrix improves the response and sensitivity of ruthenium-(II)-complex-based [7–9] and platinum-(II)-complex-based oxygen sensors [10–12]. There are many oxygen-sensitive dyes which can be used for optical oxygen sensing. Pd(II) complexes [14–20] have been used in recent years in preference to organic dye complexes with Ru(II) and Pt(II), because they can be easily excited with a compact and low-cost LED light source.

In 2008, Chu *et al.* [16] developed a very sensitive ratiometric optical fiber oxygen sensor incorporating a sol-gel matrix doped with palladium (II) meso-tetrakis(pentafluorophenyl)porphyrin (PdTFPP) as the oxygen-sensitive component and 7-amino-4-trifluoromethyl coumarin (AFC) as the reference dye. The PdTFPP-doped oxygen sensor yields a linear Stern–Volmer plot

and has a sensitivity of around 74. In 2011, Badocco *et al.* [17] used PdTFPP embedded in a polymeric matrix to produce an oxygen sensor with a sensitivity of  $I_{N_2}/I_{25\%O_2} = \sim 7$ . We present a high-performance optical fiber oxygen sensor based on PdTFPP embedded in a *n*-propyltrimethoxysilane (*n*-propyl-TriMOS)/tetraethylorthosilane (TEOS)/*n*-octyltriethoxysilane (Octyl-triEOS) composite xerogel. The experimental results show that the PdTFPP-doped *n*-propyl-TriMOS/TEOS/Octyl-triEOS oxygen sensor has a sensitivity of  $I_{N_2}/I_{100O_2} = 263$ . These results show that optical oxygen sensors based on PdTFPP have excellent sensitivity. The development of ultra-sensitive detection techniques still remains a major challenge, and there is a need for a simple, low-cost approach to their fabrication. In this study, we have chosen a Pd(II) complex (PdTFPP). Recently, the important properties of porous silica nanostructures have been receiving much research attention, especially for biology, catalysis, health sciences, and many industrial applications [21–24]. Because a high surface-to-volume ratio is an important property for optical oxygen sensors, our lab presents a highly sensitive optical oxygen sensor based on the tris(4,7-diphenyl-1,10-phenanthroline)ruthenium(II) ( $[Ru(dpp)_3]^{2+}$ ) and porous silica nanoparticles embedded in a TEOS/Octyl-triEOS composite xerogel. Experimental results show that the proposed optical fiber oxygen sensor has a higher sensitivity than one based on a Ru(II) complex immobilized in the sol-gel matrix. The proposed process enhances the sensitivity of the sensor [25].

The objective of the current study was the development of a fiber-optic oxygen sensor with improved sensitivity. It is based on a Pd(II) complex (PdTFPP) with the porous silica nanoparticles embedded in an Octyl-triEOS/TEOS sol-gel matrix which exists as a coating on the end of the optical fiber. The emission fluorescence is quenched by the presence of oxygen, and the quenching response was increased by using the surface coating proposed. The porous silica nanoparticles increase the sensing surface area per unit mass as well as the sensitivity. Results show that the proposed fiber-optic oxygen sensor can be used for applications that require high sensitivity.

## 2. Materials and Methods

### 2.1. Fabrication of Two Fiber-Optic Oxygen Sensors

The fiber-optic oxygen sensor developed in this study was fabricated using a Pd(II) complex (PdTFPP, Frontier Scientific Inc., Logan, UT, USA) and porous silica nanoparticles embedded in tetraethylorthosilane (TEOS, Sigma-Aldrich Co. LLC., St. Louis, MO, USA)/*n*-octyltriethoxysilane (Octyl-triEOS, Sigma-Aldrich Co. LLC., St. Louis, MO, USA), giving a composite xerogel which was used as a coating on the end of an optical fiber. Sensors using a Pd(II) complex embedded in a TEOS/Octyl-triEOS composite xerogel were also fabricated as a comparison. The basic steps of porous silica nanoparticle synthesis are given in the sub-sections below.

### 2.2. Synthesis of Solid Monodispersive SiO<sub>2</sub> Spheres

Solid spheres of monodispersive SiO<sub>2</sub> 50–800 nm in diameter were prepared using a slightly modified Stöber process [26]. In this typical synthesis, 1 mL of 13.7 M ammonium hydroxide was added to 4.6 mL of absolute ethanol via stirring for 10 min and designated as solution “A”. Solution “B” was prepared by adding 0.1 mL of TEOS to 0.4 mL of absolute ethanol via stirring for 10 min. Solution B was quickly added to solution A, and the resulting solution (“C”) was stirred for 2 h. Solution C was then centrifuged, and the resulting precipitate was washed with acetone until the supernatant was clear. A TEM image of the silica nanoparticles obtained is shown in Figure 1. The nanoparticles are spherical with a diameter of around 400 nm. Full details of the silica nanoparticle preparation process is presented by the current authors in [27].

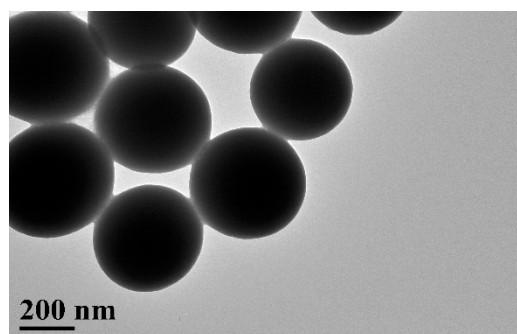


**Figure 1.** TEM image of silica nanoparticles.

### 2.3. Synthesis of Porous Silica Nanoparticles

In the typical process, 0.3 g of  $\text{SiO}_2$  spheres and 1 g of polyvinyl pyrrolidone (PVP) were added to 20 mL of water. The resulting dispersate was heated at 60 °C for 24 h via stirring. Then, 0.5 mL of NaOH (0.1 g/mL) and 1.5 mL of  $\text{NaBO}_2$  (0.1 g/mL) were added to the solution via vigorous stirring, and the mixture was kept at 30 °C for 1 h. All of the other steps of the synthesis were performed at room temperature using a technique similar to that described by Zhang *et al.* [28]. Figure 2 is a TEM image of porous silica nanoparticles synthesized using the process described above. It can be seen that the porous silica nanoparticles are spherical with a diameter of around 300 nm. The porous structure can be clearly seen as differences in electron transmission through the silica shell.

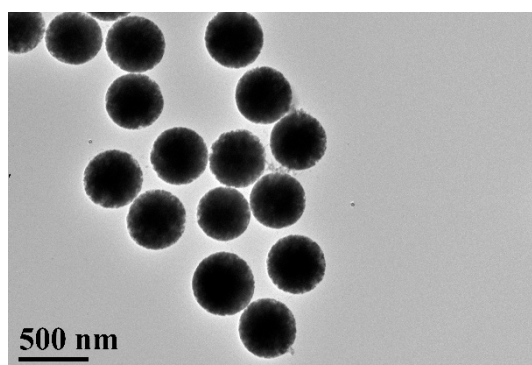


**Figure 2.** TEM image of porous silica nanoparticles.

### 2.4. The Sol-Gel Mixing and Dip-Coating Processes

The TEOS/Octyl-triEOS composite sol used as the matrix material for the optical oxygen sensors was prepared by mixing 4 mL of TEOS with 0.2 mL of Octyl-triEOS to form a precursor solution. An approach similar to that employed by Chu *et al.* [10] was used, and 1.25 mL of EtOH and 0.4 mL of 0.1 M HCl were then added to the sol to catalyze the ORMOSIL reaction. The vessel was capped and placed on a magnetic stirrer for 1 h at room temperature. During the mixing process, 0.1 mL of Triton-X-100 were added to the solution to improve the homogeneity of the silica sol, resulting in a crack-free monolith. The oxygen-sensitive dye solution was prepared by dissolving 2 mg of PdTFPP in 10 mL of EtOH. The resulting solution (1 mL) was then added to the porous silica nanoparticles and stirred for 10 min. This solution was then added to the composite sol solution. Finally, the vessel was capped and placed on the magnetic stirrer for another 10 min.

The end of a multimode optical fiber was soaked in a NaOH solution for 24 h, after which it was rinsed with copious amounts of de-ionized water and EtOH and dried at room temperature for 10 min. The composite xerogel with the porous silica nanoparticles was then deposited on one end of the fiber

in a dip-coating operation performed at a velocity of 0.25 mm/s (with a thickness usually  $<1 \mu\text{m}$ ). Finally, the coated fiber was dried at room temperature and left to stabilize under ambient conditions for 1 week.

### 2.5. Instrumentation

Figure 3 is a schematic of the experimental arrangement used to characterize the performance of the fiber-optic oxygen sensors. In the sensing experiments, the fluorescence excitation was provided by an LED (LED405E, Thorlabs, Newton, NJ, USA) with a central peak wavelength of 405 nm driven by a TGA1240 waveform generator (Thurlby Thandar Instruments Ltd, Huntingdon, UK) at 10 kHz. The oxygen sensing system consisted of a coated multimode silica glass fiber (1000/1035  $\mu\text{m}$ ) and a bifurcated optical fiber (BIF-600-UV-VIS, Ocean Optics, Dunedin, FL, USA). The relative fluorescence intensity measurements were acquired at a pressure of 101.3 kPa using a USB 4000 spectrometer (Ocean Optics).

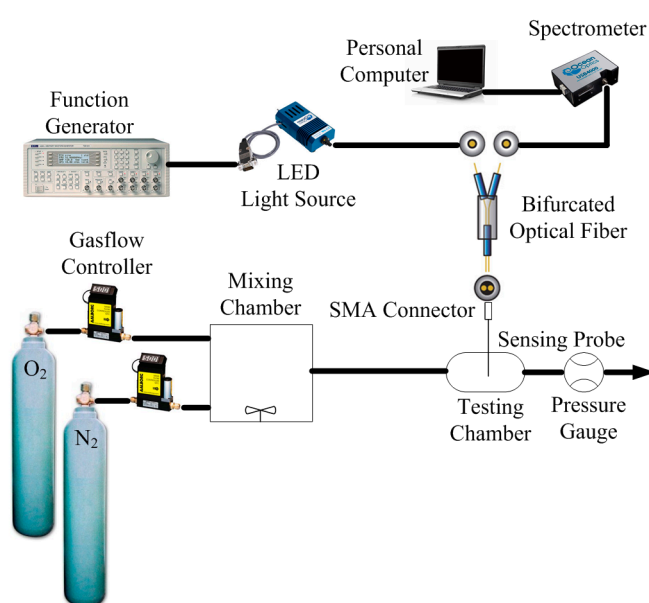
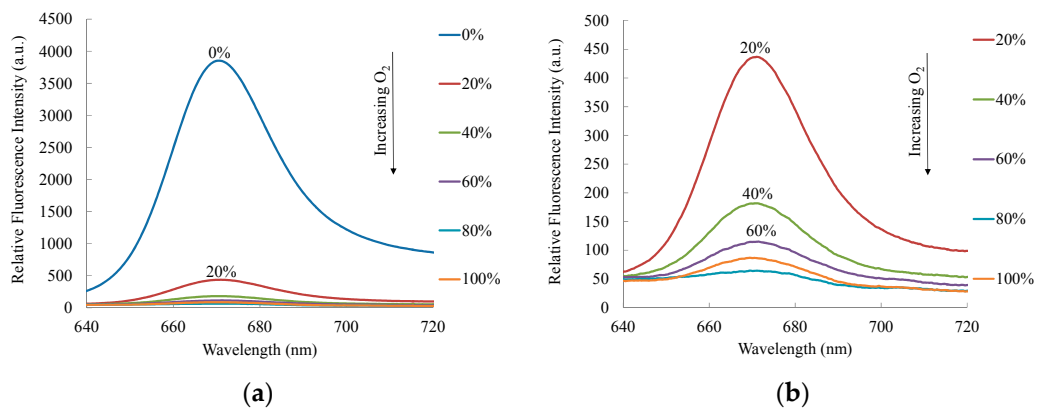


Figure 3. Schematic diagram of the experimental setup used for characterization.

## 3. Results and Discussion

The room-temperature fluorescence spectra of the two fiber-optic oxygen sensors under oxygen concentrations ranging from 0%–100% and 20%–100% are shown in Figures 4 and 5. Both sensors exhibit a strong fluorescence response at a wavelength of 670 nm. It can be seen from the figures that the relative fluorescence intensities of both sensors decrease significantly as the oxygen concentration increases. The relative fluorescence intensity of the Pd(II)-doped oxygen sensor with porous silica nanoparticles drops rapidly when oxygen concentration changes from 0%–20%, and it is clear that this sensor has high sensitivity. It also has better oxygen diffusivity and surface-area-to-volume ratio than the composite xerogel because the porous silica nanoparticles have large surface areas [21–24]. This high surface-area-to-volume ratio has the potential of providing very high sensitivity in optical sensing applications. The large specific surface area also makes these porous silica nanoparticles suitable as adsorbents for other optical sensing applications. Furthermore, the large internal surface area of the nanoparticles and the comparatively small size of the dye molecules makes it likely that all but a negligible fraction of the dye is bound to the walls of the pore channels [29].



**Figure 4.** Emission spectra of Pd(II)-doped oxygen sensor under different oxygen concentrations: (a) 0%–100% and (b) 20%–100%.

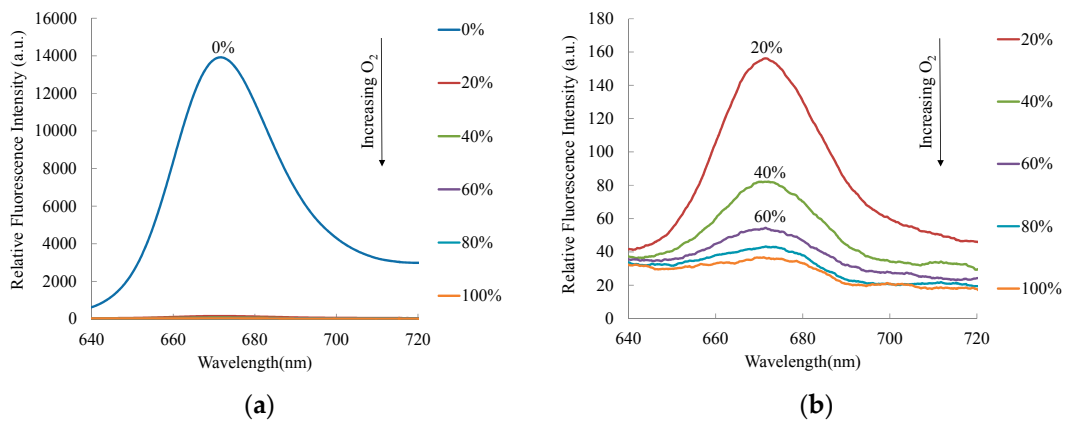


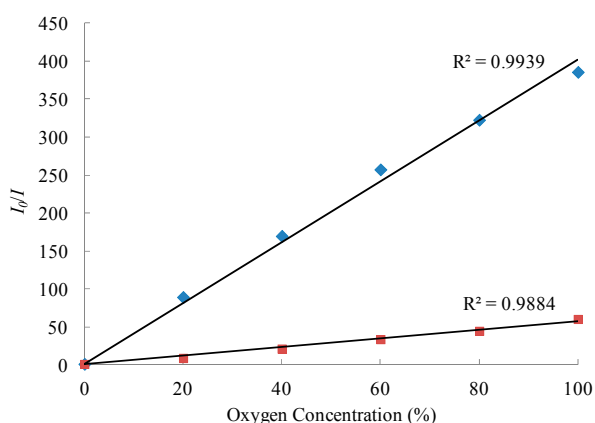
**Figure 5.** Emission spectra of Pd(II)-doped oxygen sensor with porous silica nanoparticles under different oxygen concentrations: (a) 0%–100% and (b) 20%–100%.

In a homogeneous microenvironment, quenching follows the Stern–Volmer [30] equation:

$$I_0/I = 1 + K_{SV}[O_2] \tag{1}$$

where  $I_0$  and  $I$  represent the steady-state fluorescence intensities in the absence and presence of  $O_2$ , respectively;  $K_{SV}$  is the Stern–Volmer quenching constant; and  $O_2$  is the oxygen concentration. In an ideal case, a plot of  $I_0/I$  against  $O_2$  is linear with a slope equal to  $K_{SV}$  and an intercept of unity, allowing the application of a simple single-point sensor calibration scheme.

Figure 6 presents the Stern–Volmer plots of the Pd(II)-doped oxygen sensor and Pd(II)-doped oxygen sensor with porous silica nanoparticles. These plots provide an indication of the relative sensitivities of the optical sensors to  $O_2$  quenching, and the plots are linear. The sensitivities of the optical oxygen sensors are given by the ratio  $I_{N_2}/I_{O_2}$ , where  $I_{N_2}$  and  $I_{O_2}$  represent the relative fluorescence intensities in a pure nitrogen or pure oxygen environment. It can be seen that the sensitivities of the Pd(II)-doped oxygen sensor and Pd(II)-doped oxygen sensor with porous silica nanoparticles are around 60 and 386, respectively. The sensitivity of Pd (II)-doped oxygen sensor with porous silica nanoparticles is six times higher than that of the Pd (II)-doped oxygen sensor. It is clear that the proposed processes enhance the sensitivity of optical oxygen sensors.



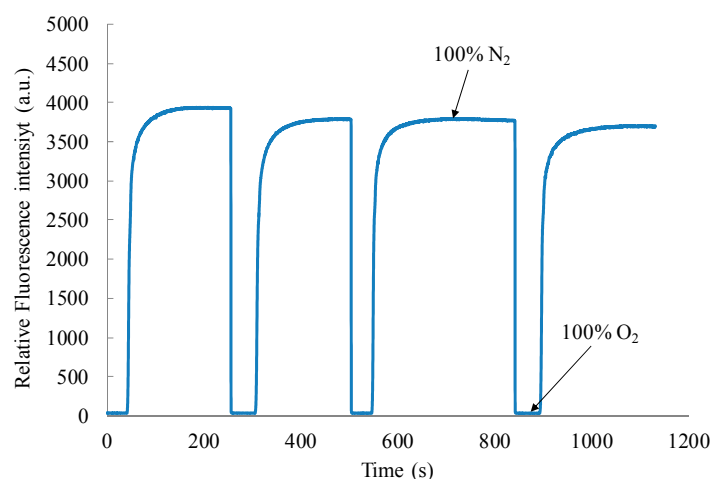
**Figure 6.** Stern–Volmer plots for Pd(II)-doped oxygen sensor (■) and Pd(II)-doped oxygen sensor with porous silica nanoparticles (◆).

Table 1 compares the performance characteristics of the current Pd(II)-doped oxygen sensors with those of representative quenchometric O<sub>2</sub> sensors fabricated using PdTFPP-doped dye in different support matrices. A comparison of the performance of the various PdTFPP-doped oxygen sensors shows that the optical sensor based on PdTFPP with porous silica nanoparticles embedded in a sol-gel matrix has a significantly higher sensitivity ( $I_{N_2}/I_{100\%O_2} \sim 386$ ) than those with a sol-gel or polymer matrix. This higher sensitivity can be attributed to the high surface-area-to-volume ratio of the dye entrapped within the porous silica nanoparticles. This improves oxygen diffusivity and enhances the quenching effect.

**Table 1.** Comparison of performance characteristics of the proposed oxygen sensor with those of existing optical oxygen sensors.

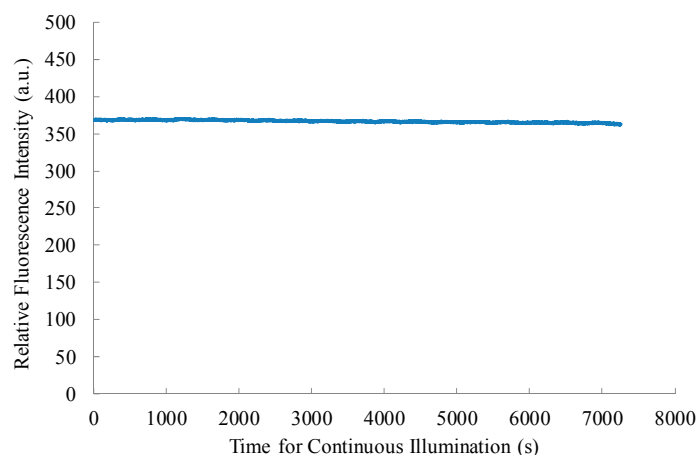
Oxygen Sensitive Dye	Support Matrix	Sensitivity	Reference
PdTFPP	silica-gel beads in silicone	$I_{N_2}/I_{100Pa,pO_2} \sim 8$	[14]
PdTFPP	polyurethane hydrogel	$I_{N_2}/I_{25\%O_2} \sim 8$	[15]
PdTFPP	TEOS/Octyl-triEOS	$I_{N_2}/I_{100\%O_2} \sim 72$	[16]
PdTFPP	PVC	$I_{N_2}/I_{25\%O_2} \sim 7$	[17]
PdTFPP	<i>n</i> -propyl-TriMOS/TEOS/Octyl-triEOS	$I_{N_2}/I_{100\%O_2} \sim 263$	[18]
PdTFPP	PEC-PCL	$I_{N_2}/I_{100\%O_2} \sim 80.6$	[19]
PdTFPP	PSU-PCL	$I_{N_2}/I_{100\%O_2} \sim 106.7$	[19]
PdTFPP and porous silica nanoparticles	TEOS/Octyl-triEOS	$I_{N_2}/I_{100\%O_2} \sim 386$	present study

Figure 7 demonstrates the typical dynamic responses of the PdTFPP-doped oxygen sensor with porous silica nanoparticles when switching between 100% O<sub>2</sub> and 100% N<sub>2</sub> environments. It can be seen that the optical sensor provides stable and reproducible signals as the environment alternates between the 100% O<sub>2</sub> and 100% N<sub>2</sub> condition. From inspection, the response time ( $t_{95}$ ; time required for 95% of the total intensity change to take place) of the PdTFPP-doped oxygen sensor with porous silica nanoparticles is found to be 2.3 s when switching from nitrogen to oxygen and 40.5 s when switching from oxygen to nitrogen. As illustrated in Figure 7, a stable and reproducible signal was obtained with the fiber-optic oxygen sensor.



**Figure 7.** Response characteristics of Pd(II)-doped oxygen sensor with porous silica nanoparticles when switching alternately between 100% N<sub>2</sub> and 100% O<sub>2</sub>.

Figure 8 shows that the photostability of proposed fiber-optic oxygen sensor. The photostability was also tested by placing the Pd(II)-doped oxygen sensor with porous silica nanoparticles with pulse irradiation with a 405-nm wavelength LED at room temperature for around 2 h. After continuous illumination for around 2 h, the relative fluorescence intensity of the fiber-optic sensor is about  $367 \pm 4$ . Figure 8 shows that the proposed sensor using PdTFPP with porous silica nanoparticles is stable.



**Figure 8.** Photostability of Pd(II)-doped oxygen sensor with porous silica nanoparticles.

#### 4. Conclusions

We have presented a highly sensitive fiber-optic oxygen sensor based on Pd(II) complex (PdTFPP) and porous silica nanoparticles embedded in a TEOS/Octyl-triEOS composite xerogel. The experimental results show that it has a linear response to oxygen concentration in the range 0%–100% and a sensitivity ( $I_{N_2}/I_{100\%O_2}$ ) of approximately 386, which is six times higher than a typical optical oxygen sensor based on the Pd(II) doped complex in a sol-gel matrix. The porous silica nanoparticles not only increase the surface area per unit mass of the sensing surface but also increase sensitivity because a substantial number of aerial oxygen molecules can penetrate the porous silica shell. This sensor can be used for applications that required high sensitivity.

**Author Contributions:** Cheng-Shane Chu conceived and designed the experiments; Jhih-Jheng Syu performed the experiments and participated in data analysis.

**Conflicts of Interest:** The authors declare no conflict of interest.

## References

1. Clark, L.C., Jr. Monitor and control of blood and tissue oxygen tensions. *Trans. Am. Soc. Artif. Intern. Organs* **1956**, *2*, 41–48.
2. Papkovsky, D.B. New oxygen sensors and their application to biosensing. *Sens. Actuators B Chem.* **1995**, *29*, 213–218. [[CrossRef](#)]
3. Demas, J.N.; Degraff, B.A.; Coleman, P.B. Oxygen sensors based on luminescence quenching. *Anal. Chem.* **1999**, *71*, 793A–800A. [[CrossRef](#)] [[PubMed](#)]
4. Tsukada, K.; Sakai, S.; Hase, K.; Minamitani, H. Development of catheter type optical oxygen sensor and applications to bioinstrumentation. *Biosens. Bioelectron.* **2003**, *18*, 1439–1445. [[CrossRef](#)]
5. Vander Donckt, E.; Camerman, B.; Herne, R.; Vandeloise, R. Fiber-optic oxygen sensor based on luminescence quenching of a Pt(II) complex embedded in polymer matrices. *Sens. Actuators B Chem.* **1996**, *32*, 121–127. [[CrossRef](#)]
6. Lee, S.K.; Okura, I. Photostable optical oxygen sensing material: Platinum tetrakis (pentafluorophenyl) porphyrin immobilized in polystyrene. *Anal. Comm.* **1997**, *34*, 185–188. [[CrossRef](#)]
7. Zhang, H.R.; Lei, B.F.; Liu, Y.L.; Liu, X.T.; Zhang, M.T.; Dong, H.W.; Xiao, Y.; Zhang, J.Y. Sol-gel-derived highly sensitive optical oxygen sensing materials using Ru(II) complex via covalent grafting strategy. *J. Nanosci. Nanotechnol.* **2014**, *14*, 4615–4621. [[CrossRef](#)] [[PubMed](#)]
8. Mill, A.; Graham, A.; O'Rourke, C. A novel, titania sol-gel derived film for luminescence-based oxygen sensing. *Sens. Actuators B Chem.* **2014**, *190*, 907–912. [[CrossRef](#)]
9. Farooq, A.; Al-jowder, R.; Narayanaswamy, R.; Azzawi, M.; Roche, P.J.R.; Whithead, D.E. Gas detection using quenching fluorescence of dye-immobilised silica nanoparticles. *Sens. Actuators B Chem.* **2013**, *183*, 230–238. [[CrossRef](#)]
10. Chu, C.S.; Lin, C.A. Optical fiber sensor for dual sensing of temperature and oxygen based on PtTFPP/CF embedded in sol-gel matrix. *Sens. Actuators B Chem.* **2014**, *195*, 259–265. [[CrossRef](#)]
11. Chu, C.S.; Lin, T.H. Ratiometric optical sensor for dual sensing of temperature and oxygen. *Sens. Actuators B Chem.* **2015**, *210*, 302–307. [[CrossRef](#)]
12. Chu, C.S.; Lin, K.Z.; Tang, Y.H. A new optical sensor for sensing oxygen based on phase shift detection. *Sens. Actuators B Chem.* **2016**, *223*, 606–612. [[CrossRef](#)]
13. McDonagh, C.; MacCraith, B.D.; McEcoy, A.K. Tailoring of sol-gel films for optical sensing of oxygen in gas and aqueous phase. *Anal. Chem.* **1998**, *70*, 45–50. [[CrossRef](#)] [[PubMed](#)]
14. Borisov, S.M.; Lehner, P.; Klimant, I. Novel optical trace oxygen sensors based on platinum(II) and palladium(II) complexes with 5,10,15,20-meso-tetrakis-(2,3,4,5,6-pentafluorophenyl)-porphyrin covalently immobilized on silica-gel particles. *Anal. Chim. Acta* **2011**, *690*, 108–115. [[CrossRef](#)] [[PubMed](#)]
15. Borisov, S.M.; Vasylevska, A.S.; Krause, C.; Wolfbeis, O.S. Composite luminescent material for dual sensing of oxygen and temperature. *Adv. Mater.* **2006**, *16*, 1536–1542. [[CrossRef](#)]
16. Chu, C.S.; Lo, Y.L. Ratiometric fiber-optic oxygen sensors based on sol-gel matrix doped with metalloporphyrin and 7-amino-4-trifluoromethyl coumarin. *Sens. Actuators B Chem.* **2008**, *134*, 711–717. [[CrossRef](#)]
17. Badocco, D.; Mondin, A.; Pastore, P. Rationalization of the behavior of a bi-label oxygen optical sensor. *Sens. Actuators B Chem.* **2011**, *158*, 54–61. [[CrossRef](#)]
18. Chu, C.S. Optical fiber oxygen sensor based on Pd(II) complex embedded in sol-gel matrix. *J. Lumin.* **2013**, *135*, 5–9. [[CrossRef](#)]
19. Xue, R.P.; Ge, C.; Richardson, K.; Palmer, A.; Viapiano, M.; Iannutti, J.L. Microscale sensing of oxygen via encapsulated porphyrin nanofibers: Effect of indicator and polymer “core” permeability. *ACS Appl. Mater. Interfaces* **2015**, *7*, 8606–8614. [[CrossRef](#)] [[PubMed](#)]
20. Chu, C.S.; Chuang, C.Y. Highly sensitive fiber-optic oxygen sensor based on palladium tetrakis (4-carboxyphenyl)porphyrin doped in ormosil. *J. Lumin.* **2014**, *154*, 475–478. [[CrossRef](#)]
21. Yin, Y.D.; Lu, Y.; Sun, Y.G.; Xia, Y.N. Silver nanowires can be directly coated with amorphous silica to generate well-controlled coaxial nanocables of silver/silica. *Nano Lett.* **2002**, *2*, 427–430. [[CrossRef](#)]

22. Zhang, T.R.; Ge, J.P.; Hu, Y.X.; Zhang, Q.; Aloni, S.; Yin, Y.D. Formation of hollow silica colloids through a spontaneous dissolution-regrowth process. *Angew. Chem. Int. Ed.* **2008**, *47*, 5806–5811. [[CrossRef](#)] [[PubMed](#)]
23. Wang, L.; Zhao, W.J.; Tan, W.H. Bioconjugated silica nanoparticles: Development and applications. *Nano Res.* **2008**, *1*, 99–115. [[CrossRef](#)]
24. Zhang, T.; Zhang, Q.; Ge, J.; Goebel, J.; Sun, M.; Yan, Y.; Liu, Y.S.; Chang, C.; Guo, J.; Yin, Y. A self templated route to hollow silica microspheres. *J. Phys. Chem. C* **2009**, *113*, 3168–3175.
25. Chu, C.S. Optical oxygen sensing properties of Ru(II) complex and porous silica nanoparticles embedded in sol-gel matrix. *Appl. Opt.* **2011**, *50*, E145–E151. [[CrossRef](#)]
26. Stöber, W.; Fink, A.; Bohn, E. Controlled growth of monodisperse silica spheres in micron size range. *J. Colloid Interface Sci.* **1968**, *26*, 62–69. [[CrossRef](#)]
27. Chu, C.S.; Lo, Y.L. Highly sensitive and linear optical fiber carbon dioxide sensor based on sol-gel matrix doped with silica particles and HPTS. *Sens. Actuators B Chem.* **2009**, *143*, 205–210. [[CrossRef](#)]
28. Zhang, Q.; Zhang, T.R.; Ge, J.P.; Yin, Y.D. Permeable silica shell through surface-protected etching. *Nano Lett.* **2008**, *8*, 2867–2871. [[CrossRef](#)] [[PubMed](#)]
29. Han, B.H.; Manners, I.; Winnik, M.A. Oxygen sensors based on mesoporous silica particles on layer-by-layer self-assembled films. *Chem. Mater.* **2005**, *17*, 3160–3171. [[CrossRef](#)]
30. Lakowicz, J.R. *Principles of Fluorescence Spectroscopy*, 2nd ed.; Kluwer Academic/Plenum Press: New York, NY, USA, 1999.



© 2016 by the authors; licensee MDPI, Basel, Switzerland. This article is an open access article distributed under the terms and conditions of the Creative Commons Attribution (CC-BY) license (<http://creativecommons.org/licenses/by/4.0/>).